

空心微瓶腔回音壁模式谐振的调谐方法及应变传感特性

蔡露^{1,3*}, 李尚文^{1,2}, 王进^{1,2}, 刘俊^{1,2}, 相夫程^{1,2}, 李忠嘉^{1,2}¹东北大学秦皇岛分校控制工程学院, 河北 秦皇岛 066004;²东北大学信息科学与工程学院, 辽宁 沈阳 110819;³东北大学秦皇岛分校河北省微纳精密光学传感与检测技术重点实验室, 河北 秦皇岛 066004

摘要 提出了一种双柄空心微瓶腔结构, 利用微纳光纤耦合激发出了回音壁模式(WGM)谐振, 通过控制轴向拉伸应变, 实现了回音壁模式的谐振波长和品质因子 Q 的调谐, 通过非对称拉锥的方式改变微腔结构, 增大了双柄微腔结构轴向拉伸对腔长和壁厚的改变量, 从而使谐振波长的调谐范围达到了 0.66 nm。所提结构在激光器、滤波器和传感检测等应用方面具有实际意义。实验中进一步探究了非对称双柄回音壁模式微腔的应变传感特性, 结果表明, WGM 谐振峰对轴向拉伸应变的灵敏度可达 0.795 pm/ $\mu\epsilon$, 分辨率小于 25 $\mu\epsilon$, 线性度达 0.999。由于回音壁模式谐振腔具有极窄的谐振峰, 该传感方法能够实现更高的传感分辨率, 为高分辨率应变传感提供了新思路。

关键词 集成光学; 回音壁模式; 空心微瓶腔; 谐振峰调谐; 应变传感

中图分类号 TN253

文献标志码 A

DOI: 10.3788/AOS231321

1 引言

近年来, 在诸多光学器件中, 光学谐振腔以其不受电磁干扰、灵敏度高、结构紧凑等优点, 受到广泛关注。其中, 有一类谐振腔被称为回音壁模式(WGM)谐振腔, 具有极高的品质因子(Q)和极小的模式体积, 因此在激光器^[1-2]、光通信^[3-4]、生物医学检测^[5-6]等领域发挥了优势。由于谐振腔和外界环境之间存在折射率差异, 光通过连续的全内反射沿着微腔的内表面传播, 当某些波长达到谐振条件时, 光被局限在微腔内以环形传播, 这种现象就是回音壁模式谐振。

随着 WGM 谐振腔研究的不断深入, 科研人员提出了多种谐振腔结构, 包括微球^[7]、微环^[8]、微盘^[9]、微管^[10]、微圆环面^[11]等。谐振腔结构通常具有高的 Q 值和小的模式体积, 其在激光器方面的应用中获得极窄的激发谱线^[1], 提高激光相干性; 在光通信领域中, 谐振腔结构可以作为窄带通滤波器、全光开关、光电调制器或分插复用器使用^[3], 有利于降低信道间的串扰。在传感领域, 极窄的谐振峰有助于获得极高的分辨率与极低的检测限, 使得谐振腔结构在物理、化学、生物等多个领域广泛应用^[5, 12-13]。在这些领域中, 谐振腔结构不同的应用情况可能对谐振峰参数有不同

的需求, 例如: 将其作为滤波器使用时, 期望带通频率可以调谐, 以满足不同的滤波要求; 将其引入激光器时, 期望激光输出波长可调, 以应用在光谱学、光学相干层析成像和干涉测量等领域。因此, 学者们提出了一系列谐振峰调谐方法, 调谐参量包括谐振峰的波长、 Q 值、耦合效率等。

谐振波长与谐振腔的折射率和尺寸直接相关。温度的变化能够用于调节微腔材料折射率和体积, 因此可以被用来调制谐振波长^[14-15]。Kavungal 等^[14]将液晶填充至毛细管中作为柱形谐振腔激发 WGM, 利用液晶材料的大热光系数, 即温度变化时液晶材料的折射率发生变化, 使谐振条件改变, 谐振波长移动, 这种方法的调制效率可达 267.5 $^{\circ}\text{C}^{-1}$ 。Shi 等^[15]通过将聚甲基丙烯酸甲酯(PMMA)材质的微球插入悬芯光纤的空腔内激发 WGM, 利用 PMMA 材质的大热光系数和热膨胀系数, 实现 1.93 nm 范围内的谐振峰波长调谐, 调谐效率可达 460 pm/K。除了直接对微腔结构加热, 还可以利用光热效应来精准控制谐振腔局部温度, 实现谐振峰的调谐。Yin 等^[16]将泵浦光注入微腔中, 以沉积在微腔表面的黑磷纳米片作为载体引发光热效应, 泵浦光功率与谐振峰波长和消光比均存在线性关系, 调谐效率分别为 0.033 nm/mW 和 0.180 dBm/mW。

收稿日期: 2023-07-27; 修回日期: 2023-09-07; 录用日期: 2023-09-20; 网络首发日期: 2023-09-28

基金项目: 国家自然科学基金(61803076)、河北省自然科学基金(F2022501028)、教育部中央高校基本科研业务费(2023GFZD002)

通信作者: *cailu@neuq.edu.cn

为了实现更高的调制速度,利用电光效应和压电效应间接地改变微腔的折射率和体积,是谐振波长调制的另一种方式^[17-18]。Liu等^[18]将压电晶体作为衬底制作了聚合物微环腔,在电场作用下,压电晶体带动微环发生形变,从而使谐振波长在0.71 nm范围内可调。

除此之外,机械调谐方法是能够大范围调控WGM谐振波长的最简单可行的方法^[19-21]。Qin等^[19]利用微瓶腔双柄拉伸造成的应力变化引起谐振腔直径的变化,从而调谐谐振峰波长,调谐效率可达 $1.7 \text{ pm}/\mu\epsilon$;Wang等^[20]利用吹气法制作聚合物微泡,通过控制吹气量来调控微腔尺寸及壁厚,实现大范围的激光调谐。

除了要实现大范围、高效率的谐振峰波长调谐外,谐振峰的Q值和耦合效率调谐也是重要的调谐参数,因此本文提出了双柄空心微腔结构,用于实现简单可行的WGM大范围调谐。双柄结构便于对微腔进行机械调谐,该结构制作工艺简单、成本低、可调谐性强;空心微腔的模式主要分布在微腔边界,因此选择空心微腔有利于提高微腔腔壁的形变能力,更易于实现对模式的控制和调整。利用石英单模光纤制作双柄空心微腔结构,激发的回音壁模式在空心腔薄壁中传播,通过控制轴向拉伸应变变量,即可调控微腔直径以及微腔壁厚,进而实现了回音壁模式的谐振波长和品质因子Q的调谐。进一步地,通过非对称拉锥的方式改变微

腔结构,增大了双柄微腔结构轴向拉伸对腔长和壁厚改变量,从而使谐振波长的调谐范围达到了0.66 nm,该方法在激光器、滤波器以及传感检测等应用方面具有实际意义。实验中进一步探究了非对称双柄回音壁模式微腔的应变传感特性,结果表明,WGM谐振峰对轴向拉伸应变的灵敏度可达 $0.795 \text{ pm}/\mu\epsilon$,分辨率小于 $25 \mu\epsilon$,线性度达0.999。由于回音壁模式谐振腔具有极窄的谐振峰,因此,该传感方法能够实现更高的传感分辨率,为高分辨率应变传感提供了新思路。

2 WGM谐振峰调谐原理

当入射光满足全反射条件时,光将会在微腔内呈多边形路径传播,并且谐振波长越短,多边形路径的边数越多。谐振腔的半径为 R ,微腔材料的折射率为 n_c ,如图1(a)所示,WGM谐振腔内的电场分布示意图如图1(b)所示。谐振腔半径 R 远大于入射波长 λ ,因此满足谐振条件的光的传播路径近似于谐振腔的周长,从而得到谐振波长的相位匹配条件为

$$\lambda_0 l = 2\pi n R, \quad (1)$$

式中: λ_0 为谐振波长; l 为角向模式数; n 为有效折射率。

当角向模式数 l 、有效折射率 n 或微腔半径 a 改变时,谐振波长会发生改变。

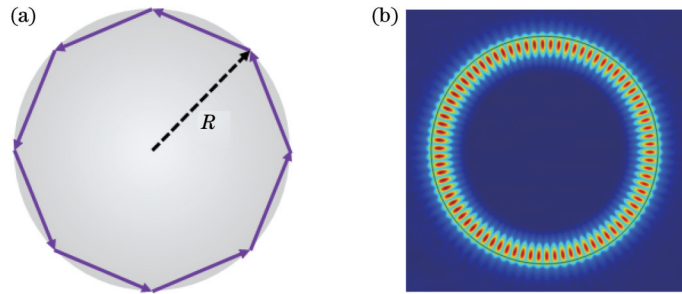


图1 回音壁模式谐振原理示意图。(a)光传播路径示意图;(b)电场分布图

Fig. 1 Principle diagram of WGM resonance. (a) Light propagation path; (b) electric field distribution

2.1 波长调控

通过控制微腔的温度和应力来调控谐振峰波长,是研究者们比较认可的两种方式。对于选定的 l 阶WGM,若改变环境温度,谐振波长的相对变化量由有效折射率和微腔半径的相对变化量决定,可以表示为

$$\frac{\Delta\lambda}{\lambda} = \frac{\Delta a}{a} + \frac{\Delta n}{n} = \frac{1}{a} \frac{\partial a}{\partial T} \Delta T + \frac{1}{n} \frac{\partial n}{\partial T} \Delta T, \quad (2)$$

式中: $\partial a/\partial T$ 是线性热膨胀系数,体现出热膨胀效应所引起的微腔半径变化; $\partial n/\partial T$ 是热光系数,体现出热光效应所引起的微腔材料折射率的变化; $\Delta\lambda$ 为谐振波长变化量; Δa 为微腔半径变化量; Δn 为微腔半径折射率; ΔT 为温度变化量。因此,可以通过直接或间接地改变谐振腔温度,调控谐振峰的波长。根据式(2),对于石英材质的谐振腔,当入射光波长在1550 nm附近

时,线性热膨胀系数约为 $5.5 \times 10^{-7} \text{ }^\circ\text{C}^{-1}$,热光系数约为 $6.3 \times 10^{-6} \text{ }^\circ\text{C}^{-1}$,温度调控效率 $\Delta\lambda/\Delta T$ 约为 $11 \text{ pm}/^\circ\text{C}$ 。

应力调控方式即通过对谐振腔施加外力使得谐振腔发生形变,同时微腔折射率也因受到弹光效应的影响而发生改变。假设微腔拉伸时轴向上各个位置的应变近似相等,则波长变化量^[22]满足

$$\frac{\Delta\lambda}{\lambda} = \frac{\Delta a}{a} + \frac{\Delta n}{n} = -(\nu + p_c)\epsilon, \quad (3)$$

式中: ν 是光纤的泊松比; p_c 是有效光弹系数; ϵ 是光纤的轴向应变。对于石英材质的光纤, $\nu \approx 0.16$, $p_c \approx 0.22$,则对1550 nm附近谐振峰的调控效率约为 $-0.58 \text{ pm}/\mu\epsilon$ 。光纤可承受的最大轴向拉伸应变可达 $2000 \mu\epsilon$,因此调控范围可达纳米级别。显然,对于石

英材质的谐振腔,应力调控效率比温度调控效率更高。本文将利用应力调控的方式进行谐振峰波长调控。

2.2 品质因子 Q 调控

品质因子 Q 值是谐振腔最重要的性能指标之一,它描述了微腔存储光的能力, Q 值越高说明微腔对光的存储能力越强。 Q 值可以定义为谐振腔内存储的光场能量与每个周期损耗能量的比值:

$$Q = \frac{-\omega W}{dW/dt}, \quad (4)$$

式中: W 表示平均存储的能量; ω 是角频率; dW/dt 表示光在腔内循环一周所损耗的能量。为了进行光谱分析,选择使用共振线宽法来进行计算,可以得到 Q 值的另一种表示方式为谐振波长与谐振峰线宽的比值:

$$Q = \frac{\omega}{\delta\omega} = \frac{\lambda}{\delta\lambda}, \quad (5)$$

式中: $\delta\lambda$ 、 $\delta\omega$ 表示谐振峰波长和频率的半峰全宽值。由式(5)可知,谐振腔的品质因子可从谐振光谱中求得,谐振腔的谐振波谷越窄,微腔的品质因子越高,其在激光器、传感器、滤波器的应用中性能越好。

考虑到谐振腔与波导耦合系统中的各种损耗,系统 Q 值^[23] 可以表示为

$$\frac{1}{Q} = \frac{1}{Q_{\text{mat}}} + \frac{1}{Q_{\text{ss}}} + \frac{1}{Q_{\text{rad}}} + \frac{1}{Q_{\text{ex}}}, \quad (6)$$

式中: $1/Q_{\text{mat}}$ 为材料吸收损耗,由制备谐振腔材料的吸光特性决定,只与材料种类和入射光波长范围相关; $1/Q_{\text{ss}}$ 为表面散射损耗,由微腔表面的均匀性和表面吸附

的污染物决定; $1/Q_{\text{rad}}$ 为辐射损耗,这部分的损耗是谐振腔的固有损耗,与微腔表面弯曲导致的光能量泄漏有关; $1/Q_{\text{ex}}$ 为耦合损耗,这是微腔和波导耦合时,二者之间倏逝场重叠较大造成的损耗,二者的场重叠越小则光损耗越小。其中,材料吸收损耗、表面散射损耗和辐射损耗组成了微腔的固有损耗 $1/Q_0$, 而耦合损耗为系统的外部损耗 $1/Q_c$ 。

对于某一石英材质的谐振腔,入射光波长确定时,材料吸收损耗和散射损耗确定,则 Q_{mat} 和 Q_{ss} 确定不变。 Q_{rad} 与材料折射率和微腔尺寸相关,当使用应力调谐方式拉伸微腔时,由式(3)可知, n 与 a 均发生变化,因此 Q_{rad} 将发生变化。 Q_{ex} 则由微腔-波导耦合系数决定,与耦合距离和耦合区倏逝场强度等因素有关,拉伸微腔时,耦合区内的微腔形态发生变化,通常表现为曲率减小,而耦合距离也将随着微腔直径的改变而发生变化。综合考虑拉伸微腔对 Q_{rad} 和 Q_{ex} 的影响,可以通过拉伸微腔来调控谐振腔的 Q 值。

3 微腔制备与实验系统搭建

由前面理论分析可知,通过在谐振腔的两端施加应力可调控谐振腔的谐振波长和 Q 值,达到调谐的目的。并且,若能使谐振腔的直径对轴向应力更灵敏,则谐振峰的调控效率更高,因此,实验中制作了双柄空心微瓶(HMB)腔,并搭建了如图2所示的WGM实验系统。空心微瓶薄壁将比实心微瓶或微球更容易因拉伸而产生形变。

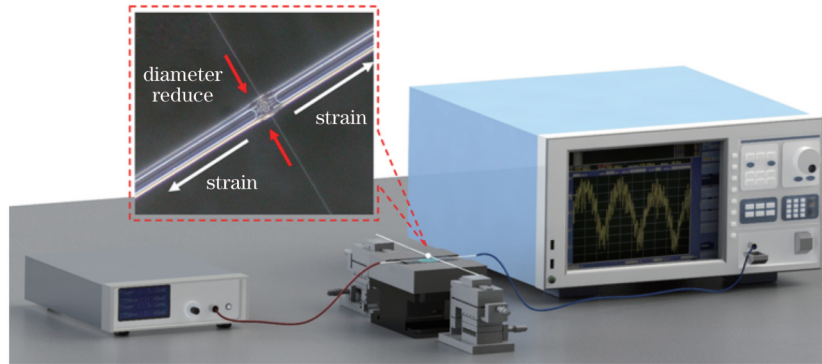


图2 WGM 光谱调谐实验系统
Fig. 2 WGM spectral tuning experiment system

通过腐蚀与熔接相结合的方式制备了如图2中插图所示的空心微瓶结构。首先将两段切割平整的掺铒光纤(芯径为 $4.5 \mu\text{m}$, NA 为 0.25)垂直插入腐蚀液中,腐蚀液是由去离子水、质量分数为 98% 的浓硫酸和氢氟酸以 2:2:3 的比例配制而成。由于 Er—O 键断裂能值小于 Si—O 键,因此纤芯的腐蚀速率更高,可腐蚀出如图3(a)所示的端面凹陷形态。紧接着,取出腐蚀后的两段掺铒光纤分别放在光纤熔接机(Fujikura S179c)的两侧电机上,通过电弧放电的方式将两段表面凹陷的掺铒光纤拼接在一起,放电时的高温使凹陷

内的空气膨胀,因此在表面张力的作用下形成微瓶的形态,最终得到如图3(b)所示的空心微瓶腔,其直径为 $107 \mu\text{m}$ 。

WGM 光谱调谐实验平台如图2所示,宽谱光源(C波段 ASE 光源, $1520 \sim 1575 \text{ nm}$)发出的光入射进锥形光纤中,在锥腰处,一部分光通过倏逝场耦合进入微腔中,激发回音壁模式谐振,其余部分的光直接通过锥形光纤,最终被光谱仪(Yokogawa AQ6370D)接收。耦合装置由两个三维位移台和一个升降台组成,升降台上固定有载玻片,并刻有相互垂直的两个凹槽,该装

置能够固定锥形光纤并约束微腔轴线与锥形光纤垂直。两个三维位移台间隔 10 cm, 分别夹持微瓶腔两端光纤, 能够精密调节锥形光纤与微瓶腔之间的耦合距离, 并能够控制微腔两端光纤的拉伸量, 从而施加轴

向应力。另外, 整个耦合过程是在一台高清电子显微镜的协助下完成的, 用于在垂直方向上观察复合型微腔与锥形光纤的耦合状态。

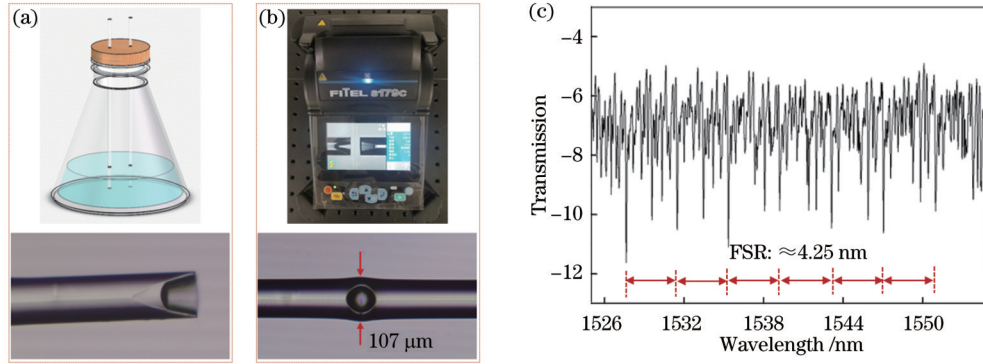


图 3 空心微瓶结构制备过程及其共振光谱。(a)化学腐蚀;(b)熔接;(c)回音壁模式共振光谱

Fig. 3 Schematic diagram of preparation and resonance spectrum of hollow microbottle structure. (a) Chemical etching; (b) fusion splicing; (c) WGM resonance spectrum

当宽谱光入射进锥形光纤后, 满足谐振波长的光会被限制在球内传播一段时间, 表现在透射光谱中即为一个一个下陷的谐振峰, 如图 3(c) 所示。由于实验中所用微瓶腔直径较大, 透射光谱中包含较多径向模式和方位角模式, 谐振峰较为密集, 自由光谱范围(FSR)约为 4.25 nm。

形光纤直接接触, 这是一种过耦合状态。之后通过拉伸微腔增加轴向应变变量, 每次改变 76 $\mu\epsilon$ 并记录谐振光谱, 观察到 1534 nm 附近的谐振峰表现出规律性的波长移动, 如图 4(a) 所示。在应变的作用下, 空心微瓶腔的轴向伸长导致谐振腔半径和折射率均减小, 从而引起了谐振峰的偏移, 且谐振峰向短波长移动, 这符合式 (3) 对谐振波长变化的描述。

实验中, 先利用三维位移台将微腔调整至轴向应变为 0, 此时为了保证实验中耦合的稳定性, 微腔与锥

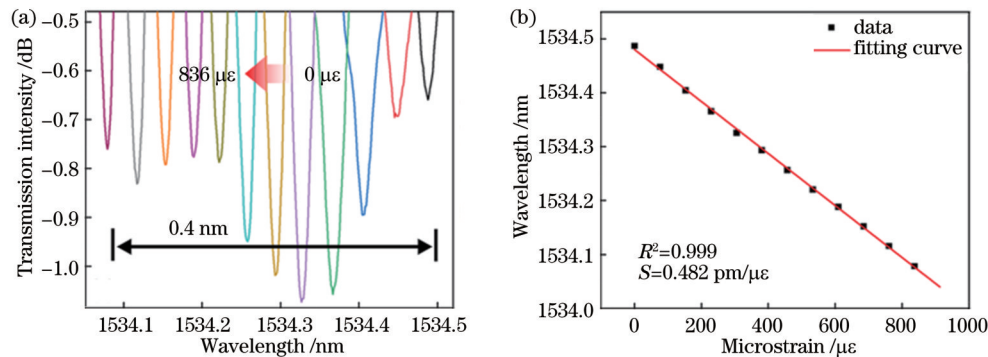


图 4 WGM 谐振波长调谐特性。(a)WGM 谐振波长的移动过程;(b)谐振峰偏移与应变变化的关系曲线

Fig. 4 Resonant wavelength tuning characteristic of WGM. (a) Shifting process of WGM resonant wavelength; (b) resonance peak shift versus strain change

图 4(b) 给出了谐振峰与应变变化的关系曲线, 可以得到谐振峰波长调谐效率为 0.482 $\text{pm}/\mu\epsilon$, WGM 谐振峰的波长调谐范围为 0.4 nm, 线性度可达 0.999。通过对谐振腔施加应变, 可以将某一谐振模式对应的波长调至期望值。另一方面, 在施加应变调谐的过程中, 某些模式对应的 Q 值也会产生变化, 如图 5(a) 所示, 这符合 2.2 节对 Q 值的分析。

的过程中, Q 值经历了先增大后减小的过程, 这与耦合损耗的变化有关。随着应变的逐渐增大, 微腔直径和耦合距离都受到调控, 微腔与锥形光纤的距离从 0 慢慢增大。同时, 回音壁模式经过了欠耦合、临界耦合和过耦合的过程, 因此透过率呈现先升高后降低的规律。这种对 Q 值的调谐作用可以应用于谐振腔的任意模式。

由图 5(b) 可以看出, 逐步增加对微瓶腔所施加的应变时, 在 1548.92 nm 处的谐振峰移动到 1548.83 nm

分析实验结果可知, 实验中轴向应力对谐振波长的调谐效率比式 (3) 得出的理论计算值小, 这一方面是

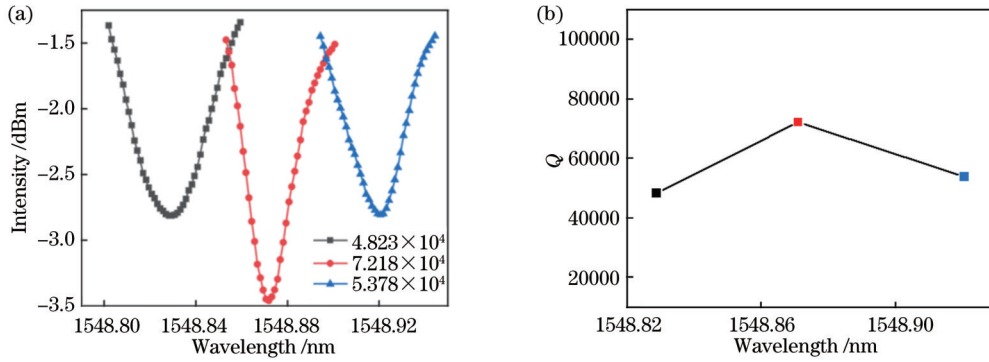


图 5 Q 值的调谐过程。(a)应变增加谐振峰蓝移;(b)施加应变使 Q 值变化

Fig. 5 Q-value tuning process. (a) Increase of strain makes resonance peak blue shift; (b) applied strain changes Q value

由于实验中光纤夹持器对光纤的夹持不够紧,夹持器与光纤之间发生了微小的相对位移,另一方面是由于两个三维位移台之间的光纤轴向应变不均匀,微瓶腔直径比两侧光纤大,使得受到拉伸后的轴向形变量小于两侧光纤。因此,为了提高调控效率,提出一种非对称结构空心微瓶腔。

4 非对称双柄微腔

由前文分析可知,采用对谐振腔施加应变的方式能够对 WGM 的光谱进行调谐。由式(3)可知,双柄微腔结构的半径对外部应变变化的灵敏度越高,结构在同样大小的外部应变条件下对 WGM 谐振波长的调谐

范围就越大,且越容易进行光谱调谐。通过对双柄微腔结构进行受力分析^[24]可知,空心谐振腔的外壁越薄时,同样大小的外部应变引起的谐振腔轴向应变越大,则谐振腔的半径变化值越大,因此制备了一种非对称空心微瓶腔(AHMB),用于谐振波长的大范围调谐。

4.1 非对称空心微瓶腔的制备

AHMB 结构制备过程以及显微镜图片如图 6 所示,在空心微瓶腔的基础上,使用熔接机在微腔一侧拉锥,使空心部分壁厚减小,从而得到更高的调控效率。用显微镜观察所制备的 AHMB 结构,可知壁厚由 $19 \mu\text{m}$ 减小到了 $6 \mu\text{m}$,微腔直径变为 $94 \mu\text{m}$ 。

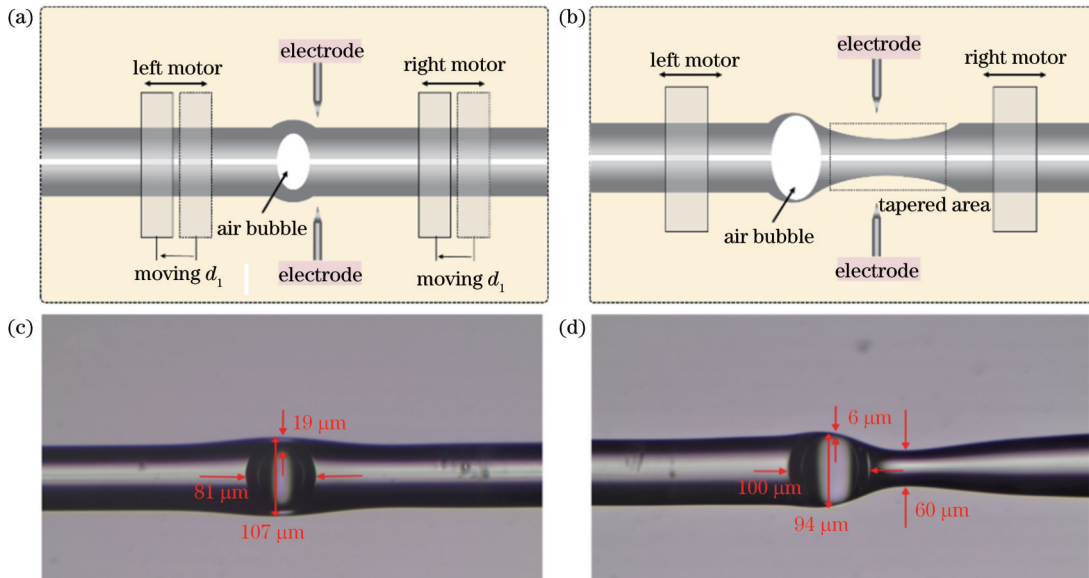


图 6 AHMB 结构的制备过程及显微镜图片。(a)左右电机同时向左移动距离 $d=60 \mu\text{m}$,使电极对准微腔右侧;(b)电极放电的同时两电机向相反方向移动,使微腔一侧形成锥形;(c)图 6(a)的显微镜图片;(d)图 6(b)的显微镜图片

Fig. 6 Preparation process and microscope images of AHMB. (a) Left and right motors are simultaneously moved toward left until distance $d=60 \mu\text{m}$, to align electrode to right of microcavity; (b) tapered region formed on one side of air-microbubble after electrodes discharge and two motors move in opposite directions simultaneously; (c) microscope image of Fig. 6(a); (d) microscope image of Fig. 6(b)

4.2 谐振波长调控实验

用图 2 所示的实验系统测试了两种微腔结构的波

长调控效率,即谐振波长的应变灵敏度,得到两种结构的应变特性如图 7 所示。由图 7 可得,AHMB 结构将

WGM 光谱谐振波长的调谐范围增大到了 0.66 nm。将两种结构的调谐灵敏度进行对比,如图 7(b)所示,通过非对称式拉锥的方式,使得外部应变对 WGM 光谱谐

振峰的调谐灵敏度增大到了 0.795 pm/ $\mu\epsilon$,并且线性度达到 0.999。若将其用作应变传感器,由于谐振峰 Q 值可达 7.218×10^4 ,应变传感分辨率可达 25 $\mu\epsilon$ 。

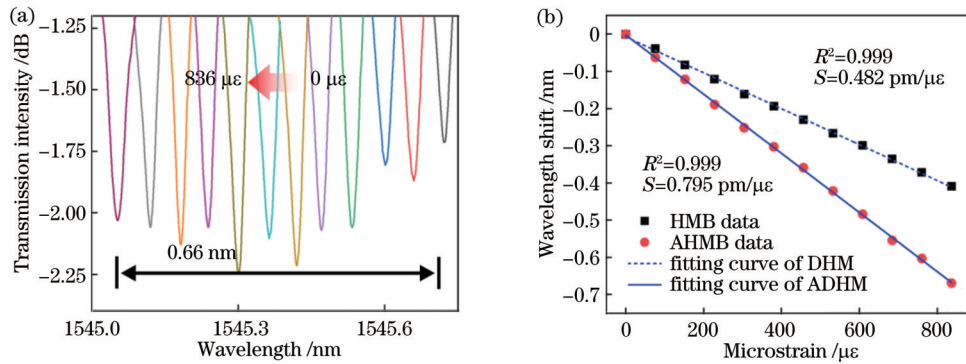


图 7 外部应变对 AHMB 结构的 WGM 谐振波长的调谐以及拉锥前后空心微瓶腔结构调谐灵敏度对比。(a)外部应变对 AHMB 结构的 WGM 谐振波长的调谐;(b)拉锥前后空心微瓶腔结构调谐灵敏度对比

Fig. 7 Tuning of WGM resonance wavelength of AHMB structure by external strain and comparison of tuning sensitivity before and after tapering. (a) Tuning of WGM resonance wavelength of AHMB structure by external strain;(b) comparison of tuning sensitivity before and after tapering

将双柄空心微瓶应变传感器与其他应变传感器进行性能(包括微腔直径、调谐范围、灵敏度、分辨率、线性度)对比。如表 1 所示,与文献[18, 25-28]相比,本

文结构的非对称空心微球在尺寸、调谐范围、灵敏度、线性度等方面都具有较好的性能。

表 1 本文中的结构与其他结构的性能对比

Table 1 Performance comparison between proposed structure and other structures

Structure	Size / μm	Tuning range / nm	Sensitivity / (pm/ $\mu\epsilon$)	Linearity	Ref. No
Polymer microring	85	0.71	—	—	[18]
Microbottle	164.5	0.106	0.085	0.9997	[25]
Microcylinder formed by polymer	490	—	0.66	0.99	[26]
Hollow-peanut-shaped microcavity	180	0.18	6.96	—	[27]
Double-tailed microsphere	160	—	0.33	—	[28]
Double-handle hollow microbottle	107	0.66	0.795	0.997	This work

5 结 论

回音壁模式的调谐在激光器、光通信、生化检测等领域有广泛应用。设计了一种由腐蚀-熔接方法制备而成的石英光纤双柄空心微瓶腔,利用轴向拉伸方法使微腔的折射率和直径发生变化,从而调谐回音壁模式的谐振波长和品质因子 Q ,调谐效率为 0.482 pm/ $\mu\epsilon$,调谐范围为 0.4 nm。在此基础上,通过非对称拉锥的方式改进了微腔结构,使微腔物理参数对轴向应变更敏感,谐振波长的调谐范围达到了 0.66 nm,调谐效率提高到 0.795 pm/ $\mu\epsilon$ 。同时,该回音壁模式调谐方法证明了微腔具有应变传感能力,分辨率低于 25 $\mu\epsilon$,线性度达 0.999,为高分辨率应变传感提供了新思路。

参 考 文 献

[1] Anashkina E A, Andrianov A V. Switchable cascade Raman lasing in a tellurite glass microresonator[J]. ACS Photonics,

2023, 10(5): 1485-1494.

- [2] Yu H M, Su X Q, Pan Y, et al. Narrow linewidth CsPbBr₃ perovskite quantum dots microsphere lasers[J]. Optical Materials, 2022, 133: 112907.
- [3] Li J W, Hu Y, Gan X F, et al. Bandwidth tunable filter based on ideal quasi-critical coupling state in WGM cavity[J]. Journal of Lightwave Technology, 2021, 39(20): 6547-6552.
- [4] Huang J S, Peng H Q. Two-channel drop filters of single photons using coupled microresonator systems[J]. International Journal of Theoretical Physics, 2023, 62(2): 42.
- [5] Reynolds T, François A, Riesen N, et al. Dynamic self-referencing approach to whispering gallery mode biosensing and its application to measurement within undiluted serum[J]. Analytical Chemistry, 2016, 88(7): 4036-4040.
- [6] Toren P, Ozgur E, Bayindir M. Real-time and selective detection of single nucleotide DNA mutations using surface engineered microtoroids[J]. Analytical Chemistry, 2015, 87(21): 10920-10926.
- [7] Neuhaus S J, Marino E, Murray C B, et al. Frequency stabilization and optically tunable lasing in colloidal quantum dot superparticles[J]. Nano Letters, 2023, 23(2): 645-651.
- [8] François A, Reynolds T, Monro T M. A fiber-tip label-free biological sensing platform: a practical approach toward *in-vivo* sensing[J]. Sensors, 2015, 15(1): 1168-1181.

- [9] Ghali H, Chibli H, Nadeau J L, et al. Real-time detection of staphylococcus aureus using whispering gallery mode optical microdisks[J]. *Biosensors*, 2016, 6(2): 20.
- [10] Luo Y H, Chen X L, Xu M Y, et al. Optofluidic glucose detection by capillary-based ring resonators[J]. *Optics & Laser Technology*, 2014, 56: 12-14.
- [11] Armani D K, Kippenberg T J, Spillane S M, et al. Ultra-high-Q toroid microcavity on a chip[J]. *Nature*, 2003, 421(6926): 925-928.
- [12] 胡建鹏, 柴明钢, 王梦宇, 等. 基于超高 Q 值回音壁模式微管腔的非接触式电流传感研究[J]. *中国激光*, 2024, 51(5): 0510002.
- Hu J P, Chai M G, Wang M Y, et al. Research of non-contact current sensor based on ultra-high Q-factor whispering-gallery mode microcapillary resonator[J]. *Chinese Journal of Lasers*, 2024, 51(5): 0510002.
- [13] 殷琦寓, 蔡露, 李尚文, 等. 在纤式回音壁模式微球谐振腔及其传感特性[J]. *光学学报*, 2023, 43(1): 0106002.
- Yin Q Y, Cai L, Li S W, et al. Microsphere resonator in fiber echo wall mode and its sensing characteristics[J]. *Acta Optica Sinica*, 2023, 43(1): 0106002.
- [14] Kavungal V, Farrell G, Wu Q, et al. Thermo-optic tuning of a packaged whispering gallery mode resonator filled with nematic liquid crystal[J]. *Optics Express*, 2018, 26(7): 8431-8442.
- [15] Shi L L, Zhu T, Huang D M, et al. Electrical thermo-optic tuning of integrated polymethyl methacrylate sphere whispering gallery mode resonator[J]. *IEEE Photonics Journal*, 2016, 8(5): 16383038.
- [16] Yin Y, Li S, Ren J, et al. All-optical modulation in black phosphorus functionalized microfiber coil resonator[J]. *Measurement Science and Technology*, 2021, 32(1): 015202.
- [17] Savchenkov A A, Ilchenko V S, Matsko A B, et al. High-order tunable filters based on a chain of coupled crystalline whispering gallery-mode resonators[J]. *IEEE Photonics Technology Letters*, 2005, 17(1): 136-138.
- [18] Liu F Y, Tong J H, Xu Z Y, et al. Electrically tunable polymer whispering-gallery-mode laser[J]. *Materials*, 2022, 15(14): 4812.
- [19] Qin H Y, Yin Y H, Ding M. Strain-induced tunable dual-bottle-shaped optical microresonator[J]. *Optics Letters*, 2019, 44(24): 6017-6020.
- [20] Wang Z, Ma Y K, Zhou H, et al. Tunable laser emissions in freestanding high-Q polymethylmethacrylate microbubbles[J]. *Laser Physics Letters*, 2020, 17(4): 045001.
- [21] Nasir M N M, Murugan G S, Zervas M N. Tunable "shallow" microbottle resonators[J]. *IEEE Photonics Technology Letters*, 2019, 31(11): 849-852.
- [22] Li E B. Sensitivity-enhanced fiber-optic strain sensor based on interference of higher order modes in circular fibers[J]. *IEEE Photonics Technology Letters*, 2007, 19(16): 1266-1268.
- [23] Gorodetsky M L, Ilchenko V S. Optical microsphere resonators: optimal coupling to high-Q whispering-gallery modes[J]. *Journal of the Optical Society of America B*, 1999, 16(1): 147-154.
- [24] Cai L, Wang J, Chen M Q, et al. A High-sensitivity strain sensor based on an unsymmetrical air-microbubble Fabry-Pérot interferometer with an ultrathin wall[J]. *Measurement*, 2021, 181: 109651.
- [25] Yin Y H, Niu Y X, Ren M X, et al. Strain sensing based on a microbottle resonator with cleaned-up spectrum[J]. *Optics Letters*, 2018, 43(19): 4715-4718.
- [26] Kavungal V, Mallik A K, Farrell G, et al. Strain-induced spectral tuning of the whispering gallery modes in a cylindrical micro-resonator formed by a polymer optical fiber[J]. *Applied Optics*, 2017, 56(5): 1339-1345.
- [27] Guo Y, Su H Y, Zhang Y D, et al. Strain-based tunable hollow-peanut-shaped optical microresonator[J]. *Optics & Laser Technology*, 2021, 139: 106762.
- [28] Yacoby E, London Y. Mechanical tuning of WGM silica microspheres and WGM-based strain gauge-geometrical considerations[J]. *Journal of Lightwave Technology*, 2022, 40(8): 2556-2560.

Adjustment Method and Strain Sensing Characteristics of Whispering Gallery Mode Resonance in Hollow Microbottle

Cai Lu^{1,3*}, Li Shangwen^{1,2}, Wang Jin^{1,2}, Liu Jun^{1,2}, Xiang Fucheng^{1,2}, Li Zhongjia^{1,2}

¹College of Control Engineering, Northeastern University at Qinhuangdao, Qinhuangdao 066004, Hebei, China;

²College of Information Science and Engineering, Northeastern University, Shenyang 110819, Liaoning, China;

³Hebei Key Laboratory of Micro-Nano Precision Optical Sensing and Measurement Technology, Northeastern University at Qinhuangdao, Qinhuangdao 066004, Hebei, China

Abstract

Objective The whispering gallery mode resonator (WGMR) has a very high quality factor and a very small mode volume, so it has great advantages in the fields of laser, optical communication, and biomedical detection. Because different applications may have different requirements for resonance peak parameters, scholars have proposed a series of resonance peak tuning methods. The tuning parameters include the wavelength of the resonance peak, Q value, coupling efficiency, etc. The resonant wavelength is directly related to the refractive index and size of the resonant cavity. In addition, the mechanical tuning method is the most simple and feasible method to control the WGM resonant wavelength in a wide range. In this paper, a double-handle hollow microbottle is proposed to achieve a simple and feasible wide-range tuning of WGM. The double-handle hollow microbottle is fabricated by using single-mode fiber, and the excited whispering gallery mode propagates in the thin wall of the hollow microbottle. By controlling the axial tensile strain, the diameter of the microcavity and the thickness of the microcavity wall can be adjusted, thereby realizing the tuning of the

resonant wavelength and the quality factor Q of the whispering gallery mode.

Methods First, the influence of controlling the temperature and stress on the resonant peak wavelength is analyzed theoretically. For the selected 1-order WGM, if the environment temperature is changed, the relative variation of the resonant wavelength is determined by the effective refractive index and the microcavity radius. The stress regulation method is to apply an external force to the resonant cavity to deform the cavity, and the refractive index of the microcavity is affected by the photoelastic effect. The quality factor Q is related to the light field energy stored in the resonant cavity and the loss energy per cycle. When the microcavity is stretched, it will affect the radiation loss and coupling loss, thereby regulating the Q value. Second, in terms of the preparation of the structure, two sections of flat Er-doped fiber are vertically inserted into the etching solution for corrosion. Then, the two sections of Er-doped fiber after corrosion are placed on the motors on both sides of the fiber fusion splicer, and the two sections of Er-doped fiber with the concave surface are spliced together by arc discharge to obtain a hollow microbottle. On the basis of the hollow microbottle, the asymmetric hollow microbottle is obtained by using the welding machine to pull the cone on the side of the microcavity. Third, the tapered fiber is fixed, and the microcavity is constrained to be perpendicular to the tapered fiber. The two three-dimensional displacement stages hold the fiber at both ends of the microbottle cavity, which can accurately adjust the coupling distance between the tapered fiber and the microbottle cavity and can control the stretching amount of the fiber at both ends of the micro-cavity, thereby applying axial stress. The whole coupling process is completed with the assistance of a high-definition electron microscope, which is used to observe the coupling state of the composite microcavity and the tapered fiber. The tuning results are observed by spectral changes.

Results and Discussions Under the action of strain, the axial elongation of the hollow microbottle leads to a decrease in the radius and refractive index of the resonant cavity, which makes the resonant peak move to the short wavelength, and it is consistent with the description of the resonant wavelength change in Eq. (3). Figure 4(b) gives the relationship curve between the resonance peak and the strain change. The wavelength tuning efficiency of the resonance peak is $0.482 \text{ pm}/\mu\epsilon$; the wavelength tuning range of the resonance peak is 0.4 nm , and the linearity can reach 0.999 . By applying strain to the resonant cavity, the wavelength corresponding to a certain resonant mode can be adjusted to the expected value. It can be seen from Fig. 5 that when the strain applied to the microbottle is gradually increased, the Q value of the resonance peak at 1548.92 nm increases first and then decreases during the process of moving to 1548.83 nm . According to the analysis in 2.2 section, it can be seen that this is related to the change of coupling loss. The tuning range of the asymmetric hollow microbottle cavity structure is increased to 0.66 nm (Fig. 7). We put the tuning sensitivity of the two structures into a figure for comparison, as shown in Fig. 7(b). By means of asymmetric tapering, the tuning sensitivity of the external strain to the WGM resonance peak increases to $0.795 \text{ pm}/\mu\epsilon$, and the linearity reaches 0.999 . If it is used as a strain sensor, the Q value of the resonance peak can reach 7.218×10^4 , and the strain sensing resolution can reach $25 \mu\epsilon$.

Conclusions In this paper, a quartz fiber double-handle hollow microbottle prepared by the etching-fusion method is designed. The refractive index and diameter of the microcavity are changed by the axial stretching method, so as to tune the resonant wavelength and quality factor Q of whispering gallery mode. The tuning efficiency is $0.482 \text{ pm}/\mu\epsilon$, and the tuning range is 0.4 nm . On this basis, the microcavity structure is improved by asymmetric tapering so that the physical parameters of the microcavity are more sensitive to axial strain. The tuning range of the resonant wavelength reaches 0.66 nm , and the tuning efficiency is increased to $0.795 \text{ pm}/\mu\epsilon$. At the same time, the whispering gallery mode tuning method proves that the microcavity has strain sensing ability; the resolution is less than $25 \mu\epsilon$, and the linearity is 0.999 , which provides a new idea for high-resolution strain sensing.

Key words integrated optics; whispering gallery mode; hollow microbottle; resonance peak tuning; strain sensing